ACS OMEGA

Open Access

http://pubs.acs.org/journal/acsodf

Article

Contamination and Cleaning of Ceramic Membrane in Phosphate Slurry Dewatering and Filtration Processes

Ran Cheng, Mingkun Wu, Juan Zhou, and Mengkui Tian*

Cite This: *ACS Omega* 2025, 10, 17917−17928

Read Online

ACCESS | Metrics & More | Article Recommendations | Supporting Information

ABSTRACT: Ceramic membrane dewatering and filtration technology is effective in reducing the water content of the phosphate slurry. However, membrane fouling remains an unavoidable issue. Herein, by investigating the mechanism of membrane contamination and developing innovative cleaning solutions, we can effectively address this issue. The main fouling form of ceramic membranes was observed to be complete blockage through analysis of the fouling process at various pollution time intervals by scanning electron microscopy (SEM) and mathematical model fitting. In addition, after cleaning severely contaminated membranes with a pollution rate of approximately 90%, a cleaning agent composed of surfactants, acid-washing agents, chelating agents, and auxiliaries was developed to address the phosphate contaminants. Owing to the combined effect of the detergent components, heavily soiled ceramic membranes can achieve a high flux recovery rate of over 90% after cleaning. This work offers new insights into ceramic membrane fouling and cleaning during phosphate slurry filtration.

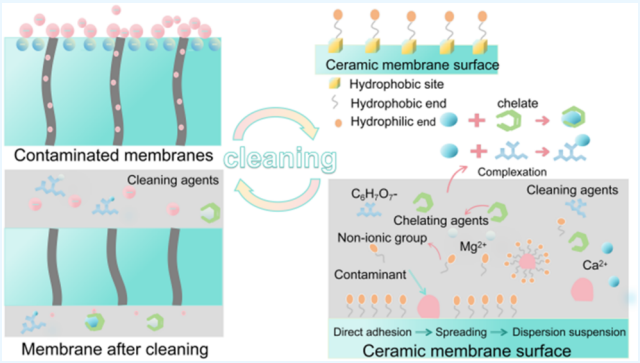

1. INTRODUCTION

The nonrenewable nature of phosphate resources has resulted in a growing interest in enhancing phosphate grades.[1−4] The beneficiation of phosphorus ore consists of comminution, separation, and dewatering steps.[5] After the phosphorus concentrate undergoes flotation treatment, the slurry exhibits a high water content, requiring dewatering and filtration.[6−8] Owing to their advantages, such as high-temperature resistance, corrosion resistance, high permeability, precise filtration, ease of regeneration and cleaning, and long service life, ceramic membranes are widely utilized in slurry dewatering processes.[9−11] Phosphorus concentrate ceramic filtration represents a typical microfiltration process, in which alumina ceramic membranes serve as a separation medium, phosphate slurry is used as the feed liquid, and the pressure difference between the interior and exterior of the membrane acts as the driving force to achieve the dewatering of the phosphate slurry. Membrane contamination is a critical issue in almost all membrane separation processes.[12−18] During the dehydration and filtration process, membrane contamination can cause blockage material to deposit on the pores on the outer surface of the membrane or inside the membrane, thereby significantly reducing the membrane's separation performance and affecting the efficient and stable filtration of ceramic membranes. Research on the mechanism of membrane blockage is a prerequisite for solving membrane pollution problems and can provide a reference for the selection of membrane cleaning methods. Therefore, there is a pressing need to elucidate the mechanism of membrane contamination and develop effective cleaning methods to promote the sustainable use of contaminated membranes.

The classical clogging model is often used to analyze the contamination clogging.[19−21] Li and others used a classical plugging mathematical model to study the fouling and cleaning of ceramic membranes during the ultrafiltration of lime sugar cane juice. The study showed that the fouling of ceramic membranes during the ultrafiltration of lime sugar cane juice is dominated by the cake layer plugging model.[20] Cai et al. systematically describe the mechanism of pollution and blockage of ceramic membranes in the water treatment process and propose that the problem of membrane pollution can be solved in two ways: pretreatment before the membrane and regeneration and cleaning after membrane pollution.[12] The determination of the membrane blockage model can provide a basis for selecting a cleaning method for the ceramic membrane. Cleaning of the contaminated ceramic membrane is required to solve the problem of regenerating the contaminated ceramic membrane. Ceramic membrane clean-

Received: February 1, 2025
Revised: April 9, 2025
Accepted: April 14, 2025
Published: April 21, 2025

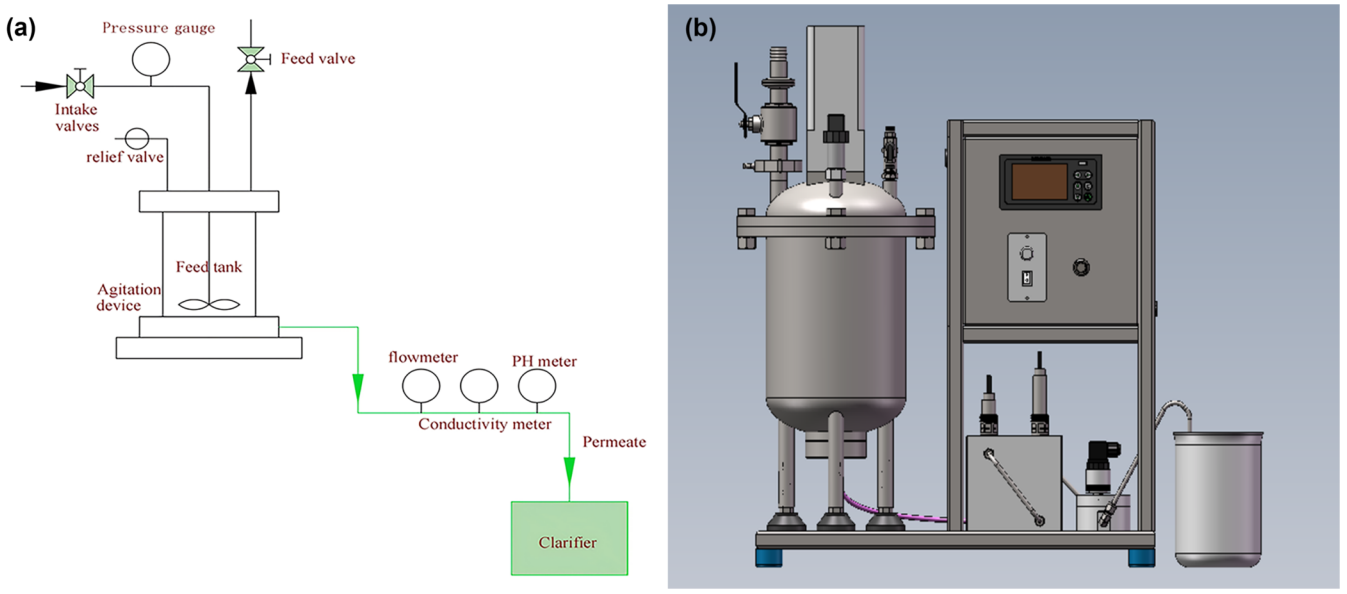

Figure 1. Process flow and physical diagram of the experimental equipment. (a) Process flow diagram. (b) Physical diagram of the device

ing methods can be categorized into physical and chemical cleaning,[22−25] in which chemical cleaning is able to remove the inner layer of clogging that cannot be removed by physical cleaning.[26−32] Currently, the phosphate concentrate dewatering and filtration process uses nitric acid, citric acid, and sulfamic acid to clean the contaminated ceramic membrane. However, previous studies exhibit the following limitations: (1) The clogging model for analyzing ceramic membrane contamination in the phosphorite slurry dewatering and filtration process is relatively underdeveloped. (2) Existing cleaning methods primarily address ceramic membrane fouling and contamination in water treatment with limited research on cleaning methods specific to phosphorite-type clogging. (3) The chemical cleaning method of contaminated ceramic membrane is relatively single, mainly relying on strong acid, strong alkali, or a combination of strong acid and alkali for cleaning. For example, nitric acid is used to clean the contaminated membrane in the phosphate concentrate dewatering and filtration process; although it can remove some of the pollutants, the corrosive and dangerous nature of nitric acid may damage the equipment and increase the safety risk. In order to achieve the goal of weak acid cleaning instead of strong acid cleaning, the use of weak acid alone is often ineffective and usually needs to be supplemented by the use of detergents, such as surfactants and chelating agents, to improve the overall efficiency of the cleaning process. However, research on multicomponent cleaning agents and their cleaning mechanisms is still limited. Therefore, there is an urgent need to develop a multicomponent, safer, and more efficient cleaning agent and to systematically and comprehensively analyze its cleaning mechanism.

In this study, phosphate slurry was selected as the model contaminant, and the time-varying curves of membrane flux under different contamination durations, as well as their linear fitting relationships with four classical membrane contamination models, were explored through both model prediction and instrumental analysis. Furthermore, a novel cleaning agent was developed, and its cleaning efficacy on the contaminated membranes was evaluated. Based on the composition of the cleaning agent, its cleaning mechanism was further investigated. This study aims to provide a theoretical foundation for the contamination and cleaning of ceramic membranes in the dewatering and filtration of phosphate slurry.

2. MATERIALS AND METHODS

2.1. Phosphate Slurry. The raw material for the phosphate rock powder was supplied by Wengfu (Group) Co., Ltd. in Guiyang, Guizhou, China, and the main components of the phosphate rock powder were fluoroapatite (Supporting Information Table S1). Before use, the phosphate powder needed to be dried at 60 °C for 10 h and sanded until there are no visible lumps. Here, we briefly describe the process of preparing the phosphate slurry solution. The specific operation was to first add 1 L of deionized water and 150 g of phosphate powder to a beaker and then stir for 1 h until the solution was evenly mixed, and no obvious layering was observed.

2.2. Membranes and Devices. An alumina ceramic membrane (Zhenjiang Ruihe Machinery Fittings Co., Ltd., Jiangsu, China) with a nominal pore size of about 5 μm was used for the dewatering and filtration of phosphate slurry. The ceramic membrane was of flat plate type with a diameter of 4 cm, a thickness of 9 mm, and a filtration area of 12.57 cm^2. The chemical reagents used in the experiments included glycolic acid ($C_2H_4O_3$, ≥98%), polyether F68 (average molecular weight 8350), fatty acid methyl ester ethoxylate (≥70%), and sodium citrate ($C_6H_5Na_3O_7$-$2H_2O$, ≥99%), which were purchased from McLean Chemical Reagents Ltd. in China.

Figure 1 illustrates the flowchart of the experimental setup. Phosphorite slurry was fed into the feed tank from the feed inlet, and the formation of precipitation was prevented by homogeneous stirring. Then, the phosphate slurry was dewatered and filtered through a ceramic membrane at a pressure of 0.07 MPa. The flow rate, PH value, and conductivity of the permeate were recorded in real time at the end of the device, and the permeate was stored in the permeate tank. During the whole process, the volume of each filtration was 1 L and the filtration pressure was 0.07 MPa.

2.3. Characterization of Membranes. The particle size distribution of the phosphorite powder was determined by

https://doi.org/10.1021/acsomega.5c01000
ACS Omega 2025, 10, 17917−17928

using a laser particle size analyzer (Malvern Mastersizer 3000+ Ultra, U.K.). The surface and cross-sectional morphologies of the ceramic membranes at different stages of contamination and after cleaning were observed by scanning electron microscopy (SEM) (TESCAN MIRA LMS, Czech Republic) and atomic force microscopy (AFM) (BRUKER Dimension Icon). A contact angle analyzer (DSA-X Plus) was used to determine the static contact angle of the ceramic membranes before and after contamination and cleaning.

2.4. Membrane Contamination Experiment and Membrane Cleaning. *2.4.1. Membrane Contamination Experiment.* In this study, 1 L of feed solution containing 150 g of phosphate rock was used for continuous dewatering and filtration in a flat alumina ceramic membrane. The feed and permeate channels of the membrane module were of the same size, and the effective membrane filtration area was 12.5 cm^2. All experiments were performed at room temperature. The contaminated membranes were removed after 4, 8, and 16 h of filtration.

2.4.2. Contaminated Membrane Cleaning Experiment. A cleaning agent was developed comprising a surfactant, a detergent chelating agent, and an acid detergent. Specifically, polyether and fatty acid methyl ester ethoxylate were utilized as surfactants, sodium citrate was employed as a rinse aid, hydroxyethylidene diphosphonic acid served as the chelating agent, and acetic acid was used as the acid rinse agent. Cleaning of membranes was performed after 4, 8, and 16 h of contamination. The removed membranes were first dried in a desiccator at 80 °C for 10 h and subsequently cleaned using a homemade detergent (100 mL). The cleaning process of the membrane included ultrasonic cleaning in a prepared cleaning agent for 120 min followed by drying in a drying oven at 80 °C for 10 h. Finally, the pure water flux of the cleaned ceramic membrane was measured.

To measure the degree of membrane contamination, we define and calculate the membrane contamination rate F as follows

$$F = \frac{J_0 - J_1}{J_0} \times 100\% \quad (1)$$

where F is the membrane contamination rate (%), J_0 is the initial unit membrane flux of the new ceramic membrane, and J_1 is the unit membrane flux of the contaminated membrane during dehydration filtration (mL/min·cm^2).

The ceramic membranes were contaminated for different periods under an operating pressure of 0.07 MPa, and the membrane contamination during the filtration process was recorded separately, specifically, the changes in the unit membrane flux, permeate conductivity, and PH after 4, 8, and 16 h of filtration. Subsequently, the membranes at different contamination periods were cleaned, and the cleaning effect of the cleaning agent was evaluated based on the membrane flux recovery rate. The calculation formula is as follows:

$$R = \frac{J_2}{J_n} \times 100\% \quad (2)$$

where R is the membrane flux recovery rate (%), J_2 is the unit pure water membrane flux (mL/min·cm^2) of the cleaned membrane, and J_n is the initial unit membrane flux (mL/min·cm^2) of the new ceramic membrane.

2.5. Fouling Blockage Modeling. The clogging filtration law is used to describe changes in flux or system pressure during dead-end filtration of porous membranes.[33] There are four types of clogging models for membrane filtration: the completely clogged model, the standard blockage model, the intermediate blockage model, and the cake layer filtration model.[34] The corresponding membrane contamination equations are in the form shown in Table 1.

Table 1. Membrane Contamination Model and Equation[a]

membrane contamination modeling	mathematical equation
completely clogged model	$\ln(J^{-1}) = \ln(J_0^{-1}) + k_b t$
standard blockage model	$J^{-1/2} = J_0^{-1/2} + k_s t$
intermediate blockage model	$J^{-1} = J_0^{-1} + k_i t$
cake layer filtration model	$J^{-2} = J_0^{-2} + k_c t$

[a] k_b is the area of pore blockage per unit flux. k_s is the cross-sectional area of decline per unit flux. k_i is the area of blocked membrane per unit flux. k_c is the area of the contamination layer formed per unit flux.

2.6. Analyzing the Cleaning Effect of Detergents through the Membrane Cleaning Effect. An increase in solution conductivity usually reflects an increase in the concentration of free ions in the solution.[35] By monitoring the change in the conductivity of the filtrate in real time, it is possible to indirectly determine whether the cleaning agent effectively removes contaminants from the membrane surface. At the same time, the real-time change of the filtrate PH can also be used as another indirect indicator to assess whether the cleaning agent has chemically reacted with the contaminants on the surface of the ceramic membrane. In order to deeply explore the cleaning effect of the cleaning agent, this paper first tested and analyzed the conductivity and PH value of the filtrate in real time during the cleaning process. Then, the effectiveness of the cleaning agent in removing the contaminants on the membrane surface was verified by comparing the contact angle change of the contaminated ceramic membrane before and after cleaning, combined with SEM and AFM images.

2.7. Analyze the Cleaning Mechanism from the Composition of the Cleaning Agent. The components of cleaning agents include surfactants, chelating agents, acidic cleaning agents, and pickling aids. Their role in the cleaning process was analyzed in depth by incorporating the properties of the selected reagents. Specifically, analyzing the interactions and possible reactions between the cleaning agent and solid clogging can help us understand the cleaning mechanism in order to reveal its action more fully.

3. RESULTS AND DISCUSSION

3.1. Pollution from Phosphate Mines. Figure 2 demonstrates the variation of unit membrane flux and conductivity of ceramic membranes during three repetitive dewatering and filtration experiments of a phosphate slurry over 16 h.

During the experiment, the unit membrane flux decreased from 38.45 to 4.43 mL/min·cm^2. After 4 h of continuous dehydration and filtration, the contamination rate of the membrane was about 30%. After 8 h of continuous dehydration and filtration, the contamination rate increased to 60%, and after 16 h, the contamination rate approached 90%. The real-time conductivity of the permeate showed a steady decrease. The conductivity remained stable at about 0.7

https://doi.org/10.1021/acsomega.5c01000
ACS Omega 2025, 10, 17917−17928

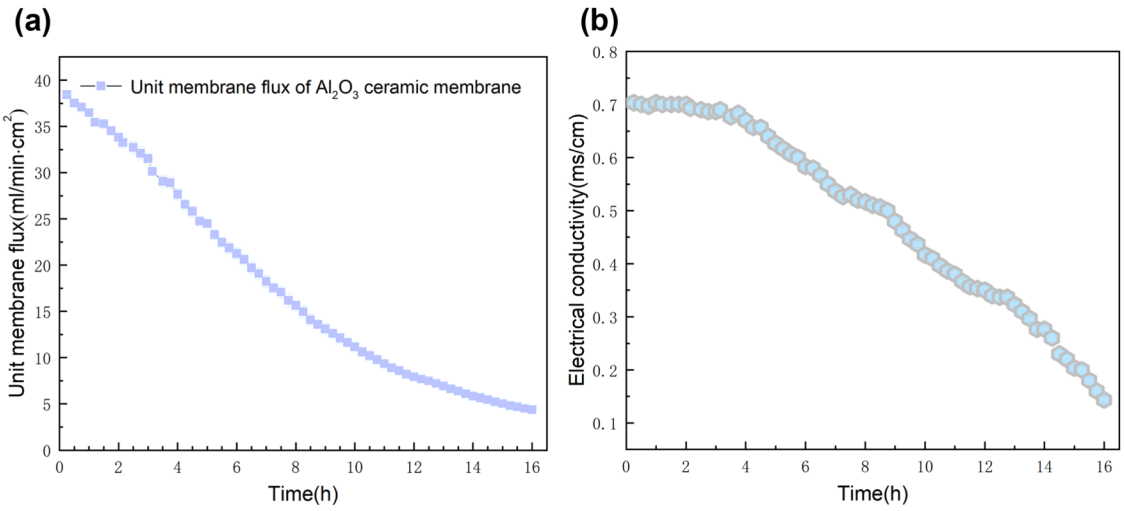

Figure 2. Variation curves of unit membrane flux and conductivity with time for continuous filtration for 16 h. (a) Time variation curve of unit membrane flux. (b) Time variation curve of conductivity

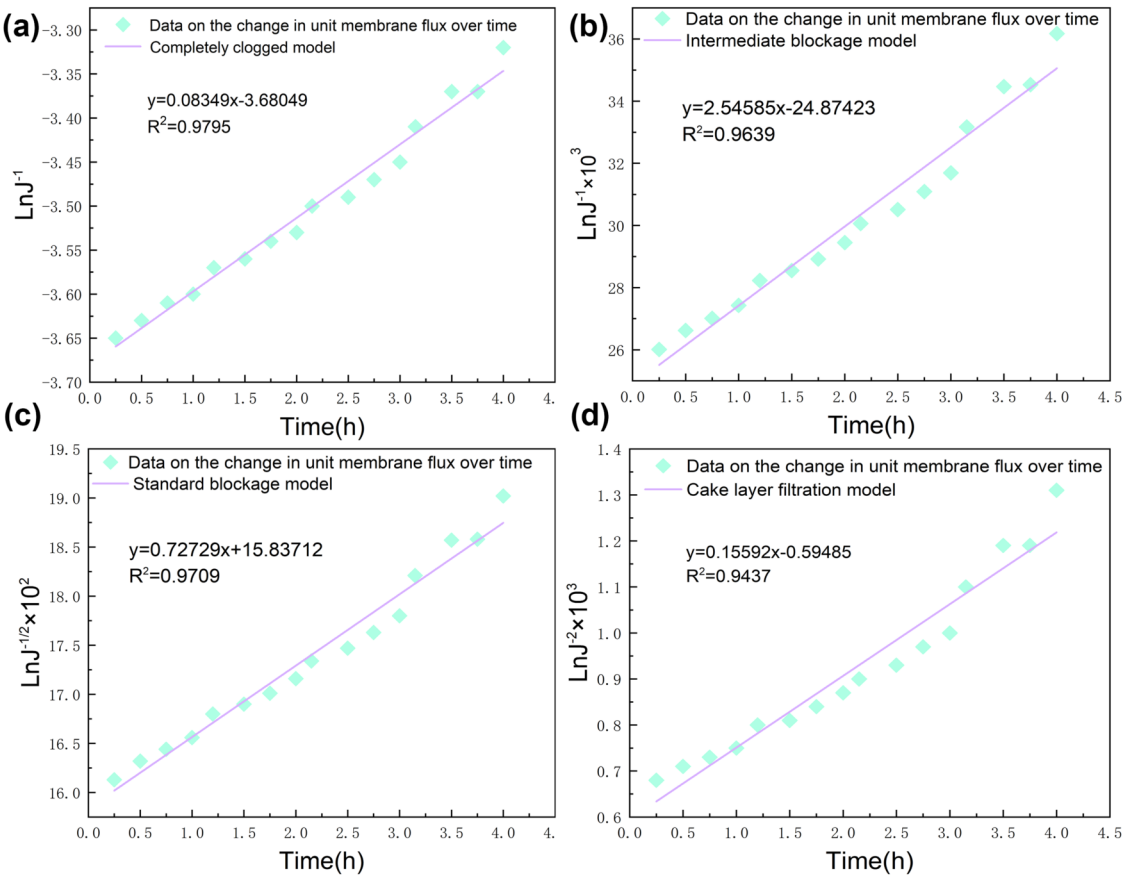

Figure 3. Fitting curves of continuous filtration for 4 h with four filtration models. (a) Completely clogged model. (b) Intermediate blockage model. (c) Standard blockage model. (d) Cake layer filtration model.

mS/cm for the first 4 h and then decreased by about 25% after 8 h of continuous filtration. Finally, it was found that the conductivity decreased by about 80% after 16 h of continuous filtration. Based on the change curves of unit membrane flux and conductivity, the different degrees of membrane contamination were defined as mild contamination after 4 h (membrane contamination rate of about 30%), moderate contamination after 8 h (membrane contamination rate of about 60%), and heavy contamination after 16 h (membrane contamination rate of about 90%).

3.2. Analysis of Membrane Contamination Mechanism by Filtration Clogging Model. In this study, the fouling process was systematically analyzed for different continuous contamination durations to reveal the fouling mechanism, and the changes in membrane flux during the dewatering and filtration of the phosphate slurry by ceramic membranes were fitted to different contamination models. The

https://doi.org/10.1021/acsomega.5c01000
ACS Omega 2025, 10, 17917−17928

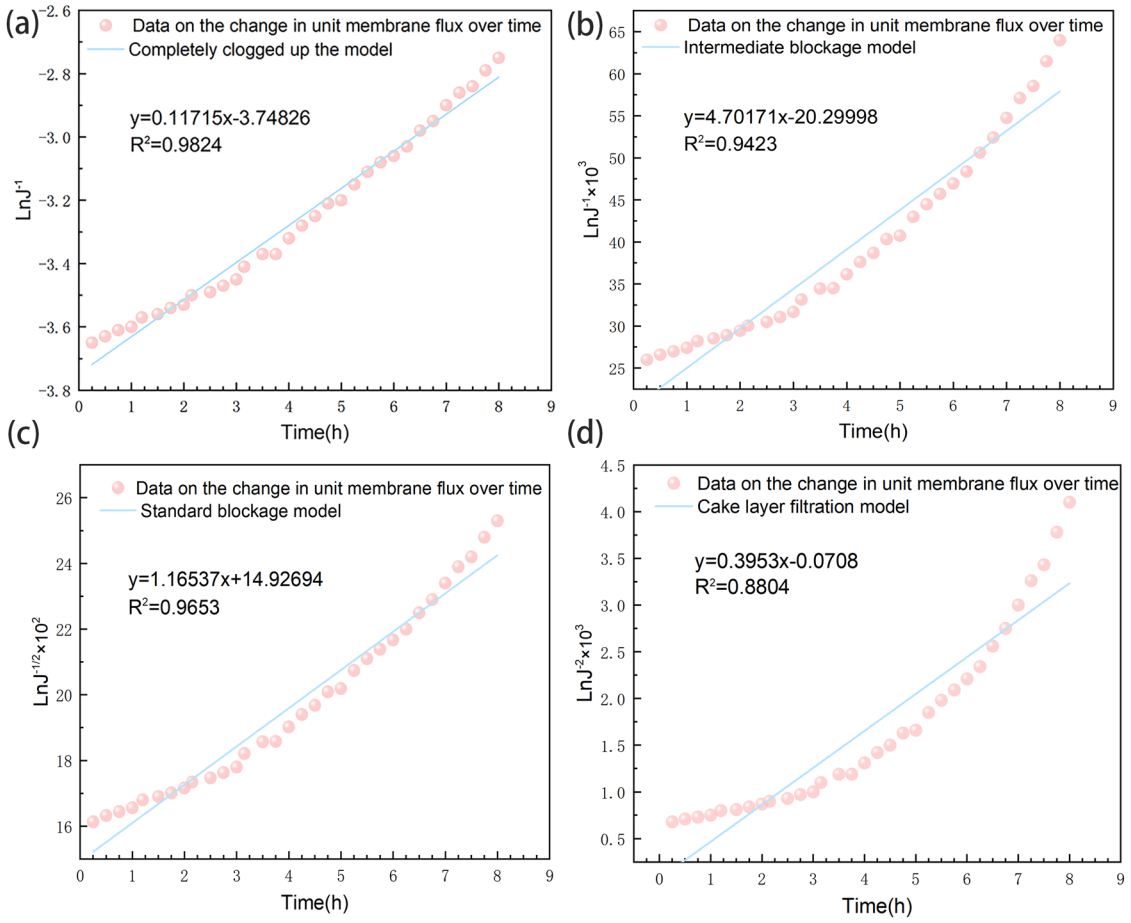

Figure 4. Fitting curves of continuous filtration for 8 h with four filtration models. (a) Completely clogged model. (b) Intermediate blockage model. (c) Standard blockage model. (d) Cake layer filtration model

models employed include the completely clogged model, standard blockage model, intermediate blockage model, and cake layer filtration model. The mathematical equations for each model are presented in Table 1, and additional details regarding these models can be found in the prior study.[36] The results of fitting the membrane flux data to the different fouling models for 4, 8, and 16 h filtration processes are shown in Figures 3, 4, and 5, respectively.

The linear correlation coefficients of each clogging model for different time periods of the fouling process are as follows: for the 4 h fouling process, the linear correlation coefficients of the completely clogged model, the intermediate blockage model, the standard blockage model, and the filtration model of the cake layer are 0.9795, 0.9639, 0.9709, and 0.9437, respectively (Figure 3). For the 8 h fouling process, the linear correlation coefficients of the completely clogged model, the standard clogging for the 8 h fouling process, the linear correlation coefficients of the completely clogged model, the intermediate blockage model, the standard blockage model, and the filtration model of the cake layer, were 0.9824, 0.9423, 0.9653, and 0.8804, respectively (Figure 4). For the 16 h fouling process, the linear correlation coefficients of the completely clogged model, the intermediate blockage model, the standard blockage model, and the filtration model of the cake layer were 0.9926, 0.8958, 0.9585, and 0.7369, respectively (Figure 5).

These results suggested that the contamination process of ceramic membrane dewatering and filtration of phosphate slurry is mainly dominated by a complete clogging model, followed by the standard blockage model, and there are also an intermediate blockage model and cake layer filtration model involved. This also reflected the fact that the membrane fouling process was the result of the combined action of multiple forms of pollution. The attenuation of flux may be caused by a combination of various pollution mechanisms, and the relative importance of different pollution mechanisms may change over time. The outer surface of the contaminated membrane will form some large pores that are similar in size to the dirt particles, mainly caused by the uneven pore size distribution and the inconsistent size of the membrane pore channels. As the contamination time increased, the linear correlation coefficient of the completely clogged model gradually approached 1, indicating that the pores of the ceramic membrane were gradually blocked and the phosphate particles gradually accumulated in the membrane pores, resulting in increased membrane contamination and eventually complete blockage of the pores. However, in the actual process, the type of membrane clogging changes with the actual changes in production and the dominance of the model may change accordingly.

3.3. Analysis of Membrane Contamination Mechanism by Phosphorite Particle Size Distribution. In order to obtain the particle size distribution of the phosphorite, the laser particle size analyzer was used in this study to determine the particle distribution of the phosphorite without obvious agglomeration after grinding, as shown in Figure 6. According

https://doi.org/10.1021/acsomega.5c01000
ACS Omega 2025, 10, 17917−17928

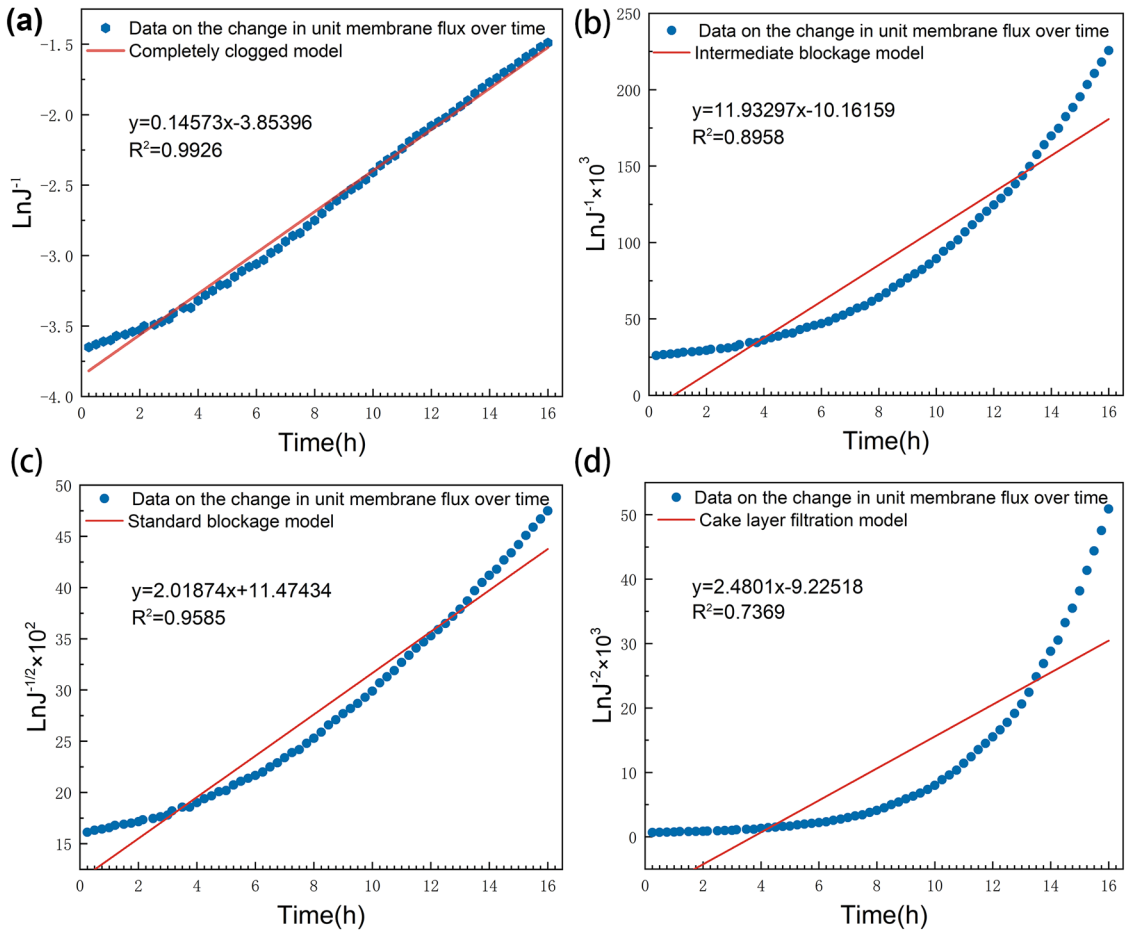

Figure 5. Fitting curves of continuous filtration for 16 h with four filtration models. (a) Completely clogged model. (b) Intermediate blockage model. (c) Standard blockage model. (d) Cake layer filtration model.

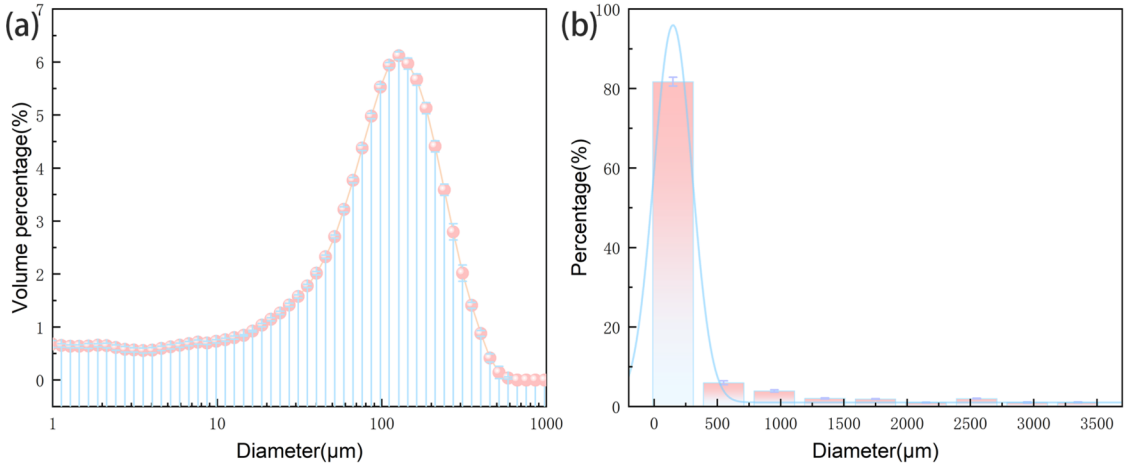

Figure 6. Phosphorus powder particle size distribution curve and particle size distribution frequency histogram. (a) Phosphorus powder particle size distribution curve. (b) Phosphorus powder particle size distribution frequency histogram.

to the particle size distribution curve, the particle size range of phosphorite extends from 1 to 3500 μm, with the majority of particles concentrated in the 20 to 500 μm range. The frequency histogram of the particle size distribution indicates that particles within the range of 0−500 μm represent approximately 80% of the total. The nominal pore size of the ceramic membrane is 5 μm. As the contamination time increases, large phosphorite particles gradually accumulate on the membrane surface, resulting in the obstruction of the membrane pores; meanwhile, smaller particles enter the membrane pores and accumulate, progressively obstructing the pores, which ultimately leads to a decline in membrane flux. This process elucidates the mechanism of ceramic membrane contamination. The particle size in the feed liquid directly affected the type of membrane fouling. Specifically, particles smaller than the nominal pore size of the membrane

https://doi.org/10.1021/acsomega.5c01000
ACS Omega 2025, 10, 17917−17928

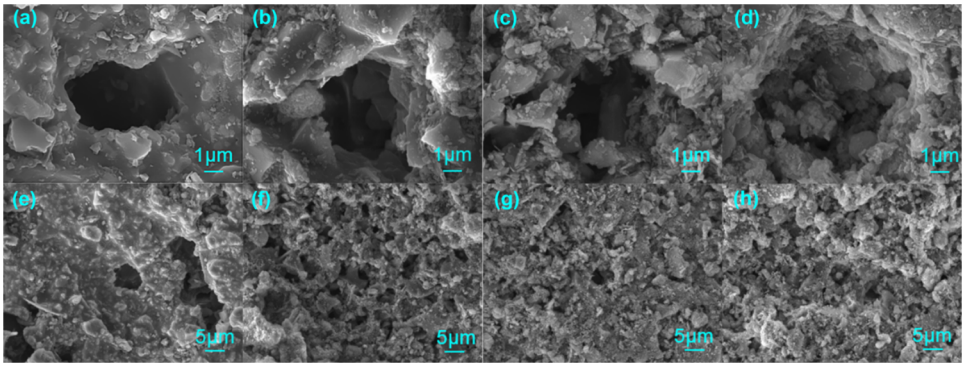

Figure 7. SEM comparison of ceramic membrane pores and surfaces with different contamination time lengths. (a) New ceramic membrane pores. (b) 4h contaminated ceramic membrane pores. (c) 8 h contaminated ceramic membrane pores. (d) 16 h contaminated ceramic membrane pores. (e) New ceramic membrane surface. (f) 4 h contaminated ceramic membrane surface. (g) 8 h contaminated ceramic membrane surface. (h) 16 h contaminated ceramic membrane surface.

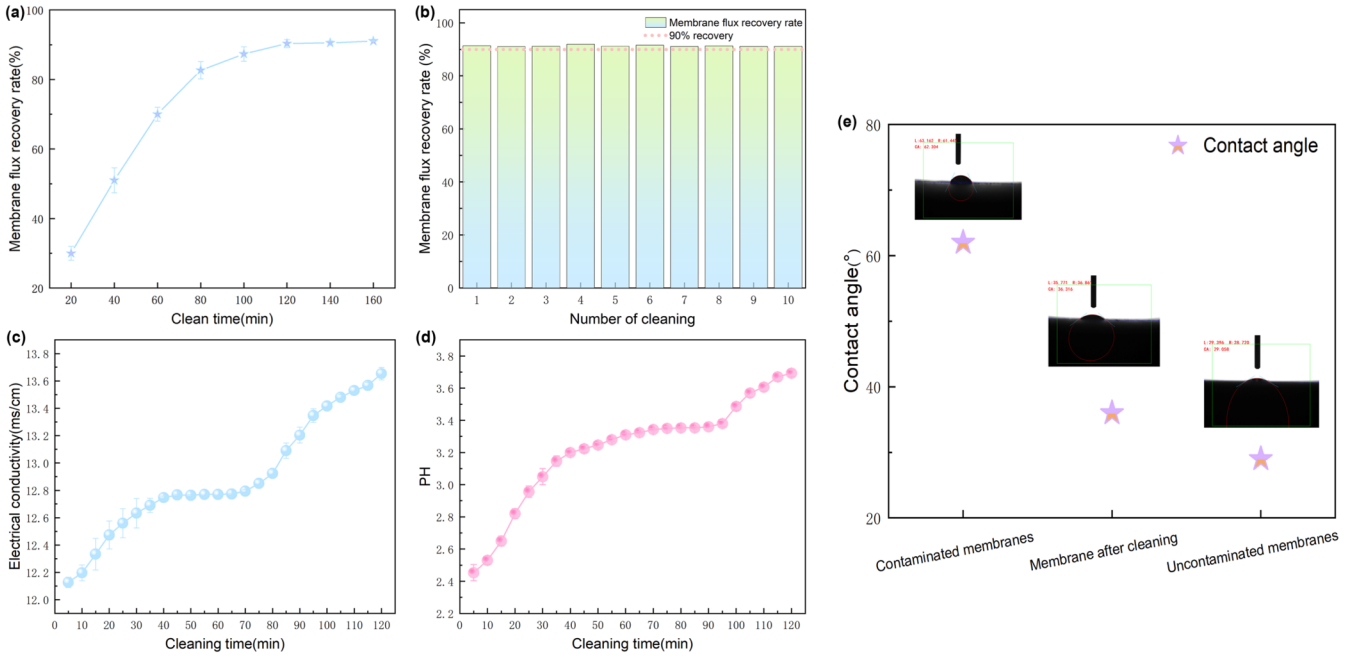

Figure 8. Ceramic membrane cleaning effect graph. (a) Membrane flux recovery rate with cleaning time. (b) Recovery curve of membrane flux after repeated cleaning of a heavily contaminated membrane. (c) Time variation curve of conductivity of filtrate during the cleaning process. (d) PH curve of the filtrate with time during the cleaning process. (e) Comparison of contact angle before and after membrane cleaning.

caused narrowing of the pore channels, particles of similar size caused standard clogging, and particles larger than the membrane pores promoted complete clogging, contributing to the formation of a filter cake layer. Compared to the intermediate blockage model and the cake layer filtration model, the completely clogged model and the standard blockage model showed better agreement with the measured data. Due to the presence of numerous particles larger than the membrane pores in the feed solution, these particles tended to clog the pores of the ceramic membrane.

The mechanism of ceramic membrane contamination during the dewatering and filtration of phosphate slurry was verified through SEM observations of membrane pore contamination at different times (4, 8, and 16 h), as well as on a new ceramic membrane. As shown in the SEM results in Figure 7, after 4 h of contamination, the membrane pores were partially blocked, and the pore diameter was slightly reduced. When the contamination time was 8 h, the accumulation of contaminated particles increased, causing most of the membrane pores to be blocked and only a small amount of pore structure could be seen on the membrane surface. After 16 h of contamination, the accumulation of contaminated particles reached saturation, the membrane pores were completely blocked and large particles of contaminants severely blocked the pores. This phenomenon is consistent with the theory of a complete pore blockage.

3.4. Membrane Cleaning Effect. We cleaned heavily contaminated ceramic membranes after 16 h of continuous contamination, i.e., membranes with a flux reduction of about 90%. The main components of phosphate minerals were analyzed, and it was determined that the contaminants were primarily fluorapatite and dolomite (Supporting Information Figure S1). Acidic cleaners were chosen because of their combination of phosphate minerals and the properties of the calcium and magnesium compounds. Cleaning experiments were conducted on contaminated membranes, which exhibited

https://doi.org/10.1021/acsomega.5c01000
ACS Omega 2025, 10, 17917−17928

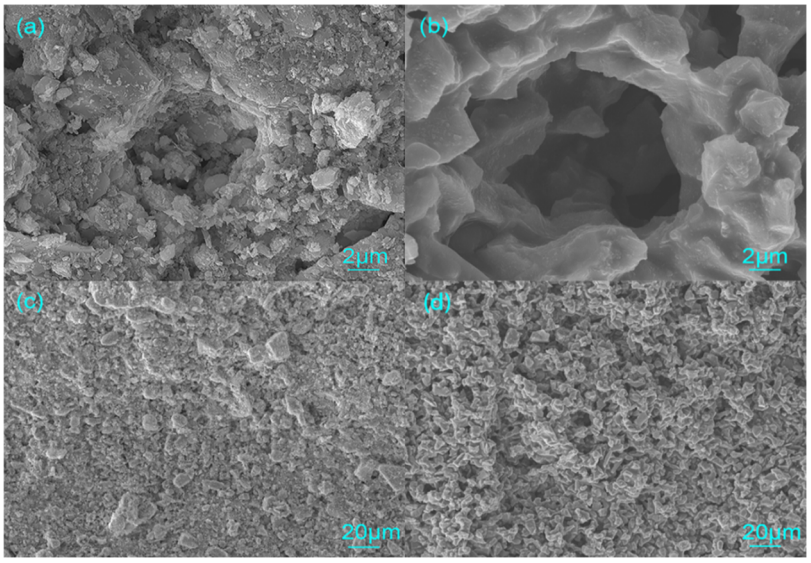

Figure 9. SEM comparison of ceramic membrane before and after cleaning for heavy contamination. (a) Ceramic membrane pores before cleaning. (b) Ceramic membrane pores after cleaning. (c) Ceramic membrane surface before cleaning. (d) Ceramic membrane surface after cleaning.

approximately a 90% reduction in membrane flux over various durations. As shown in Figure 8a, the membrane flux recovery remains stable at approximately 90% after 120 min of cleaning. To evaluate the cleaning effect, we repeated the cleaning experiments on the contaminated membranes with about a 90% decrease in membrane flux. After configuring the cleaning solution, the contaminated membrane was cleaned by an ultrasonic cleaning method for 120 min. During this process, we recorded the change in the pure water flux of the membrane before and after cleaning. By calculating the recovery rate of the membrane flux, we further analyzed the repeatability of the cleaning effect. According to Figure 8b, the flux recovery rate for all membranes exceeds 90%, indicating that the detergent developed has excellent and stable cleaning power.

3.4.1. Conductivity Analysis during the Cleaning Phase. To study the change in conductivity with time during membrane cleaning, the experimental setup of Figure 1(b) was used. The prepared cleaning solution was injected into the material tank and pressurized to 0.07 MPa for filtration and cleaning. The conductivity of the membrane filtrate was monitored in real time at the right end of the device, and the data was collected. The conductivity of the membrane-filtered liquid was monitored in real time, and the data were subsequently collected. The change curve of the real-time conductivity of the cleaning solution as a function of the cleaning time is presented in Figure 8c. Initially, the conductivity of the cleaning solution is approximately 12.1 mS/cm, after 120 min of cleaning, it increases to approximately 13.7 mS/cm. This result suggested that the glycolic acid in the cleaning agent might have reacted chemically with fluorapatite and dolomite. For fluorapatite clogs, glycolic acid formed a complex with calcium ions in fluorapatite through its carboxyl group to produce calcium ethanoate, and in addition, the amino group in glycolic acid may react with phosphate in fluorapatite to form organophosphates. For dolomite plugs, the carboxyl group in glycolic acid combines with calcium and magnesium ions to form calcium ethanoate and magnesium ethanoate, respectively. At the same time, glycolic acid may promote the dissolution of fluorapatite and dolomite, releasing carbon dioxide, calcium ions, and phosphate ions. These chemical reactions helped some of the contaminants to be removed from the membrane pores, and the conductivity of the membrane solution gradually increased as the cleaning solution flowed out.

3.4.2. PH Analysis of the Cleaning Phase. To investigate the temporal changes in the PH of the cleaning solution during the membrane cleaning process, real-time PH data were acquired for the filtered liquid. The curve depicting the PH value of the filtered solution as a function of the cleaning time is shown in Figure 8-d. The results indicate that the PH value increases gradually with an extension of the cleaning time, suggesting that the hydrogen ion concentration in the surface cleaning agent filtrate decreases over the course of the cleaning process. This phenomenon may be due to the reaction of the hydrogen ions in the cleaning agent with the calcium and magnesium compounds, which dissolved some of the blockage and thus consumed the hydrogen ions.

3.4.3. Changes in Membrane Contact Angle before and after Cleaning. The hydrophilicity of the membrane surface significantly influences the separation efficiency and fouling resistance of the membrane. The wettability of the membrane is typically assessed by measuring the water contact angle of the modified membrane. The cleaning efficiency can be evaluated by comparing the water contact angles of the membrane before, after, and after cleaning. As shown in Figure 8-e, the contact angle of the membrane increases significantly after contamination, which can be attributed to the blockage of the membrane pores by contaminants, leading to a decrease in the membrane's hydrophilicity. After cleaning, the contact angle of the membrane improved significantly, indicating that the cleaning process effectively unclogged the membrane pores and restored its hydrophilicity, thereby improving the separation performance.

3.4.4. Comparative Analysis of SEM and AFM before and after Membrane Cleaning. It is shown in Figure 9 that the comparison of SEM images before and after membrane cleaning indicates a significant reduction in the blockages within the pore channels, an improvement in the membrane flux, and an enhancement in the separation efficiency.

https://doi.org/10.1021/acsomega.5c01000
ACS Omega 2025, 10, 17917−17928

Moreover, the quantity of clogged material adhering to the surface of the cleaned membrane was substantially reduced, further corroborating the effectiveness of the cleaning process.

Ceramic membranes gradually undergo contamination during use due to electrostatic interactions and concentration polarization. Contaminants may clog the membrane pores, which leads to a reduction in membrane surface roughness, thereby diminishing separation efficiency and shortening the membrane's service life. The cleaning effect of the heavily contaminated membrane was further evaluated by using AFM, as shown in Figure 10, which compares AFM images of the membrane surface before and after cleaning with those of an uncontaminated membrane. The results showed that the average surface roughness (Ra) of the new ceramic membrane, the heavily contaminated membrane and the membrane after cleaning with the self-developed cleaning agent were 49.6, 24.5, and 49.3 nm, respectively. This data indicated that the surface roughness of the ceramic membrane was effectively restored after cleaning, which further verified the effectiveness of the cleaning agent.

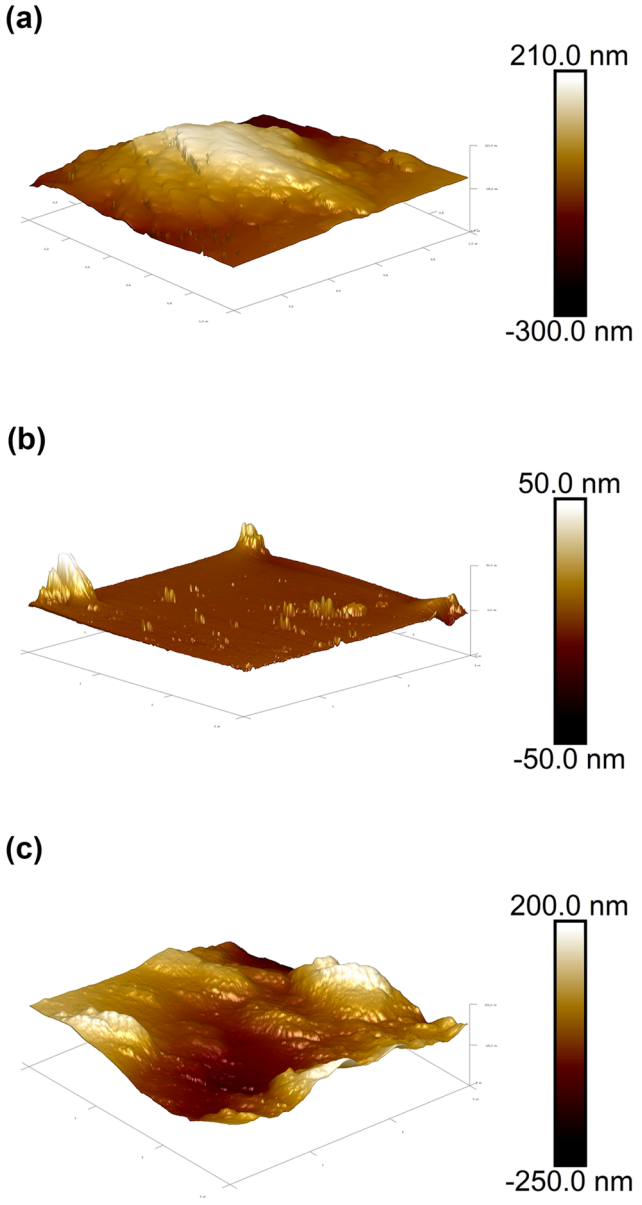

Figure 10. 3D morphology AFM image of ceramic membrane surface. (a) Uncontaminated membrane. (b) Heavily contaminated membrane. (c) Cleaned membrane.

3.5. Membrane Cleaning Mechanism. The solid fouling removal process is typically divided into three stages: in the first stage, solid fouling attaches directly to the membrane surface. In the second stage, the detergent unfolds at the solid−solid interface between the contaminant and the membrane surface, with the process being facilitated by the detergent's penetration into the tiny gaps of the capillaries at the solid−solid interface. In the third stage, the solid fouling is dispersed and suspended in the detergent. The orthogonal experiment (Supporting Information Tables S2−S4) on cleaning agents showed that surfactants had the greatest effect on cleaning solid dirt, followed by builders and chelating agents, while the effect of acid cleaners was minimal. Based on the high significance of each component, the membrane was cleaned by arranging the components in order of priority, and the results are presented in Figure 11. The experimental results

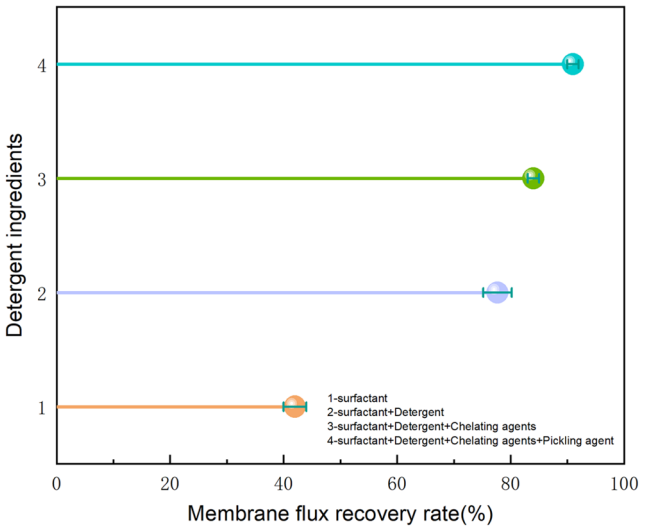

Figure 11. Cleaning effect of each component of the cleaning agent individually.

showed that the contribution of the surfactant to membrane flux recovery was about 45%, while the contribution of acid wash additives was about 40%. In contrast, the contributions of the chelating agent and acid wash additive to membrane flux recovery were 8 and 7%, respectively. These results indirectly indicated that surfactants and acid wash additives were significantly more effective than chelating agents and acid detergents in removing membrane blockage. The above results were consistent with the analysis of the orthogonal experiments.

3.5.1. Cleaning Mechanisms of Surfactants. After the ceramic membrane becomes contaminated, a significant amount of clogging material is deposited on its surface, including substances like dolomite and fluorapatite, which are hydrophobic, leading to the formation of numerous hydrophobic sites on the membrane. When surfactants are introduced into the cleaning agent, their molecular structure exhibits amphoteric characteristics, with hydrophilic groups at one end and hydrophobic groups at the other.[37,38] The hydrophobic groups of the surfactant adsorb at the hydro-

https://doi.org/10.1021/acsomega.5c01000
ACS Omega 2025, 10, 17917−17928

phobic points on the surface of the ceramic membrane, thereby improving the hydrophilicity of the membrane. Polyether and fatty acid methyl ester ethoxylates, as typical low-foaming nonionic surfactants, exhibit high stability in addition to favorable biodegradability. They do not ionize in aqueous solutions and are unaffected by strong electrolytes, strong acids, strong bases, or calcium and magnesium ions in hard water.[39] When the surfactant is dissolved in the washing solution and penetrates into the crevice, the hydrophobic groups of the surfactant are adsorbed onto the surface of the ceramic membrane and the clogging material, respectively, while the hydrophilic groups are extended into the detergent to form a monomolecular adsorption layer. This adsorptive film renders the solid dirt surface more hydrophilic,[40] which improves the compatibility between the detergent and the ceramic membrane and the clogged surface.[41,42] This process encourages the cleaning agent to spread over the solid−solid interface between the ceramic membrane and the clogging material, forming a liquid film. This film converts the solid−solid interface between the clogging material and the ceramic membrane surface into a solid−liquid interface, thereby facilitating the removal of the clogging material.

3.5.2. Acid Detergent, Detergent Aid, and Chelating Agent Cleaning Mechanisms. The main components of the blockage are fluorapatite and dolomite, where fluorapatite belongs to calcium fluorophosphate minerals, and dolomite is mainly composed of calcium carbonate and magnesium carbonate.[6] The addition of hydroxyacetic acid can effectively dissolve calcium and magnesium salts, thus realizing the descaling effect. In addition, glycolic acid has low corrosiveness to the ceramic membrane, and the safety risk in the chemical cleaning process is small. As the pollutants and the ceramic membrane surface are negatively charged, in contact between the two, electrostatic repulsion can effectively slow down membrane contamination. The addition of sodium citrate as a rinse aid can not only effectively buffer the PH value of the cleaning agent but also has a strong complexing ability, which can complex with Ca^{2+}, Mg^{2+} and other metal ions,[43−45] reduce the concentration of these metal ions in the cleaning agent, thus promoting the dissolution of calcium and magnesium microsoluble substances. The cations in the feed solution interact with the negative charges on the surface of the substance, thus exacerbating the formation of contamination. In order to effectively alleviate this problem, the chelating agent 1-hydroxyethylidene-1,1-diphosphonic acid hydroxyethylidene diphosphonic acid is able to significantly chelate hardness ions such as Ca^{2+}, Mg^{2+}, and other ions in the feed solution, in particular by forming a stable hexacyclic chelate with Ca^{2+},[46,47] thereby preventing crystallization and deposition of these ions and reducing the dirt formation The chelating agent not only has good scale inhibition effect but also shows obvious solubility limitation effect.

4. CONCLUSIONS

This paper studied the contamination mechanism of ceramic membranes during the dewatering and filtration of a phosphate slurry and the cleaning methods. The results showed that ceramic membranes were contaminated to varying degrees over time during the filtration of phosphate slurry, affecting the membrane's filtration performance. In response to the contamination problem, this article also discussed effective cleaning techniques to restore the permeability of the membrane and extend its service life.

1. By analyzing the changes in membrane flux and conductivity, it was observed that the membrane contamination rates were 30% (mild), 60% (moderate), and 90% (severe) after contamination periods of 4, 8, and 16 h, respectively. Combining mathematical modeling and SEM, the study indicated that ceramic membranes in phosphate slurry dewatering and filtration are primarily affected by complete and standard clogging models, with intermediate clogging and cake layer clogging models also contributing. Overall, membrane contamination results from the interplay of multiple mechanisms.
2. In this study, a cleaning agent was developed with the main components including surfactants (polyether and fatty acid methyl ester ethoxylates), acid detergent (glycolic acid), acid detergent additive (sodium citrate), and chelating agent (hydroxyethylidene diphosphonic acid). The cleaner was used to clean heavily contaminated ceramic membranes, and the membrane flux recovery rate exceeded 90% after 120 min of cleaning, which indicated its high reproducibility and effectiveness.
3. This study explored the cleaning mechanism of each component of the cleaning agent. The solid fouling removal process involves three stages: adhesion, spreading, and dispersion. Surfactants facilitated the spreading of the cleaning agent on the membrane surface and the effective detachment of blockages by enhancing the hydrophilicity of the contaminants. Acid detergents dissolved calcium and magnesium salts, while acid detergent additives adjusted the PH and complexed $Ca^{2+}$and Mg^{2+}. Chelating agents efficiently chelated the hardness ions in the feed solution. The synergistic action of these components ensured the efficient cleaning of contaminated ceramic membranes.

■ ASSOCIATED CONTENT

Supporting Information

The Supporting Information is available free of charge at https://pubs.acs.org/doi/10.1021/acsomega.5c01000.

Clogging composition determination data supplement: XRF testing of phosphate slurries; XRD analysis of clogged material; orthogonal experiments: table of orthogonal experimental design for detergent formulation; orthogonal experimental data of cleaning agent formulations; and data analysis of orthogonal experiments on detergent formulations (PDF)

■ AUTHOR INFORMATION

Corresponding Author

Mengkui Tian − *School of Chemistry and Chemical Engineering, Guizhou University, Guiyang 550025, P. R. China;* orcid.org/0000-0001-5376-8353; Email: tianmk78@126.com

Authors

Ran Cheng − *School of Chemistry and Chemical Engineering, Guizhou University, Guiyang 550025, P. R. China*

Mingkun Wu − *School of Chemistry and Chemical Engineering, Guizhou University, Guiyang 550025, P. R. China;* orcid.org/0000-0003-4215-2507

https://doi.org/10.1021/acsomega.5c01000
ACS Omega 2025, 10, 17917−17928

Juan Zhou − *School of Chemistry and Chemical Engineering, Guizhou University, Guiyang 550025, P. R. China*

Complete contact information is available at: https://pubs.acs.org/10.1021/acsomega.5c01000

Author Contributions

R.C.: contributed ideas, methodology, investigation, data curation, writing—original draft. M.W.: contributed ideas to support the whole work, data curation, and visualization. J.Z.: contributed to data curation and investigation. M.T.: contributed to formal analysis, funding acquisition, resources, and supervision.

Notes

The authors declare no competing financial interest.

■ ACKNOWLEDGMENTS

This work is supported by the National Natural Science Foundation of China (22162007), the Science and Technology Supporting Project of Guizhou Province ([2021]480), the Science and Technology Supporting Project of Guizhou Province ([2023]379), and Project from Guizhou Institute of Innovation and development of dual-carbon and new energy technologies (DCRE-2023-05).

■ REFERENCES

(1) Wang, B.; Zhou, Z.; Xu, D.; Wu, J.; Yang, X.; Zhang, Z.; Yan, Z. A new enrichment method of medium−low grade phosphate ore with high silicon content. *Miner. Eng.* **2022**, *181*, No. 107548.

(2) Aleksandrova, T.; Elbendari, A.; Nikolaeva, N. Beneficiation of a Low-grade Phosphate Ore Using a Reverse Flotation Technique. *Miner. Process. Extr. Metall. Rev.* **2022**, *43* (1), 22−27.

(3) Aarab, I.; Derqaoui, M.; Amari, K. E.; Yaacoubi, A.; Abidi, A.; Etahiri, A.; Baçaoui, A. Flotation Tendency Assessment Through DOE: Case of Low-Grade Moroccan Phosphate Ore. *Min., Metall., Explor.* **2022**, *39* (4), 1721−1741.

(4) Ma, Y.; Fan, H.; Khan, D.; Zhang, F.; Zhang, H.; Gao, J.; Wen, H.; He, L.; Wei, C.; Liu, Z.; Deng, Y. Tracing provenance of phosphorite in the Shifang phosphorite deposit: Insights from the genesis of detrital zircon. *Ore Geol. Rev.* **2024**, *170*, No. 106143.

(5) Yu, L.; Yu, P.; Bai, S. A Critical Review on the Flotation Reagents for Phosphate Ore Beneficiation. *Minerals* **2024**, *14* (8), 828−850.

(6) Zhou, F.; Liu, Q.; Liu, X.; Li, W.; Feng, J.; Chi, R.-a. Surface Electrical Behaviors of Apatite, Dolomite, Quartz, and Phosphate Ore. *Front. Mater.* **2020**, *7*, No. 35.

(7) Joseph-Soly, S.; Asamoah, R. K.; Skinner, W.; Addai-Mensah, J. Superabsorbent dewatering of refractory gold concentrate slurries. *Adv. Powder Technol.* **2020**, *31* (8), 3168−3176.

(8) Panayotova, M. Control of Non-Ferrous Metal-Sulfide Minerals' Flotation via Pulp Potential. *Minerals* **2023**, *13* (12), 1512−1555.

(9) Ramlow, H.; Ferreira, R. K. M.; Marangoni, C.; Machado, R. A. F. Ceramic membranes applied to membrane distillation: A comprehensive review. *Int. J. Appl. Ceram. Technol.* **2019**, *16* (6), 2161−2172.

(10) Loutou, M.; Misrar, W.; Koudad, M.; Mansori, M.; Grase, L.; Favotto, C.; Taha, Y.; Hakkou, R. Phosphate Mine Tailing Recycling in Membrane Filter Manufacturing: Microstructure and Filtration Suitability. *Minerals* **2019**, *9* (5), 318−335.

(11) Zhang, Z.; Bao, Y.; Sun, X.; Chen, K.; Zhou, M.; He, L.; Huang, Q.; Huang, Z.; Chai, Z.; Song, Y. Mesoporous Polymer-Derived Ceramic Membranes for Water Purification via a Self-Sacrificed Template. *ACS Omega* **2020**, *5* (19), 11100−11105.

(12) Cai, C.; Sun, W.; He, S.; Zhang, Y.; Wang, X. Ceramic membrane fouling mechanisms and control for water treatment. *Front. Environ. Sci. Eng.* **2023**, *17* (10), 126−140.

(13) Tian, J.; Pan, H.; Bai, Z.; Huang, R.; Zheng, X.; Gao, S. Alleviated membrane fouling of corundum ceramic membrane in MBR: As compared with alumina membrane. *J. Environ. Chem. Eng.* **2022**, *10* (6), No. 108949.

(14) Jiang, T.; Tian, T.; Guan, Y.-F.; Yu, H.-Q. Contrasting behaviors of pre-ozonation on ceramic membrane biofouling: Early stage vs late stage. *Water Res.* **2022**, *220*, No. 118702.

(15) Meng, S.; Zhang, M.; Yao, M.; Qiu, Z.; Hong, Y.; Lan, W.; Xia, H.; Jin, X. Membrane Fouling and Performance of Flat Ceramic Membranes in the Application of Drinking Water Purification. *Water* **2019**, *11* (12), 2606−2621.

(16) Qiao, Y.; Han, X.; Chen, F.; Sun, C.; Xu, L.; Liu, R.; Shen, X. Control behavior of pretreatment on ceramic membrane fouling caused by different organic substances. *J. Environ. Chem. Eng.* **2024**, *12* (1), No. 111884.

(17) Zhao, Y.-x.; Li, P.; Li, R.-h.; Li, X.-y. Characterization and mitigation of the fouling of flat-sheet ceramic membranes for direct filtration of the coagulated domestic wastewater. *J. Hazard. Mater.* **2020**, *385*, No. 121557.

(18) Li, P.; Yang, C.; Sun, F.; Li, X.-y. Fabrication of conductive ceramic membranes for electrically assisted fouling control during membrane filtration for wastewater treatment. *Chemosphere* **2021**, *280*, No. 130794.

(19) Todisco, F.; Vergni, L.; Ceppitelli, R. Modelling the dynamics of seal formation and pore clogging in the soil and its effect on infiltration using membrane fouling models. *J. Hydrol.* **2023**, *618*, No. 129208.

(20) Li, W.; Ling, G.; Lei, F.; Li, N.; Peng, W.; Li, K.; Lu, H.; Hang, F.; Zhang, Y. Ceramic membrane fouling and cleaning during ultrafiltration of limed sugarcane juice. *Sep. Purif. Technol.* **2018**, *190*, 9−24.

(21) Rafryanto, A. F.; Ramadina, Z. D. P.; Nur'aini, S.; Arrosyid, B. H.; Zulfi, A.; Rochman, N. T.; Noviyanto, A.; Arramel. High Recovery of Ceramic Membrane Cleaning Remediation by Ozone Nanobubble Technology. *ACS Omega* **2024**, *9* (10), 11484−11493.

(22) Bazán, M.; Carpintero-Tepole, V.; Brito-de la Fuente, E.; Drioli, E.; Ascanio, G. On the use of ultrasonic dental scaler tips as cleaning technique of microfiltration ceramic membranes. *Ultrasonics* **2020**, *101*, No. 106035.

(23) Fang, K.; Chen, W.; Liu, C.; Lin, D.; Nie, J.; Du, X.; Luo, Y. Chemical cleaning enhanced birnessite functional layer formed in gravity driven ceramic membrane for manganese-containing water purification. *Sep. Purif. Technol.* **2025**, *359*, No. 130801.

(24) Sun, H.; Liu, Y. Chemical Cleaning-Triggered Release of Dissolved Organic Matter from a Sludge Suspension in a Ceramic Membrane Bioreactor: A Potential Membrane Foulant. *ACS ES&T Water* **2021**, *1* (12), 2497−2503.

(25) Atallah, C.; Mortazavi, S.; Tremblay, A. Y.; Doiron, A. In-Process Steam Cleaning of Ceramic Membranes Used in the Treatment of Oil Sands Produced Water. *Ind. Eng. Chem. Res.* **2019**, *58* (33), 15232−15243.

(26) Yang, J.; Li, X.; Wei, M.; Li, J.; Li, G.; Liu, Y. Base-activated persulfate strategy for ceramic membrane cleaning after treatment of natural surface water. *Chem. Eng. Res. Des.* **2023**, *194*, 245−255.

(27) Wang, F.; Zhang, S.; Jiao, W.; Chen, J.; Zhao, S.; Ma, G.; Liu, G. Study on pickling technology to control fouling of ceramic membrane treating secondary treated effluent. *Water Sci. Technol.* **2022**, *86* (7), 1719−1732.

(28) Bai, S.; Han, J.; Ao, N.; Ya, R.; Ding, W. Scaling and cleaning of silica scales on reverse osmosis membrane: Effective removal and degradation mechanisms utilizing gallic acid. *Chemosphere* **2024**, *352*, No. 141427.

(29) Xie, S.; Wong, N. H.; Sunarso, J.; Guo, Q.; Hou, C.; Pang, Z.; Peng, Y. Cleaning mechanism of gypsum scaling in hydrophobic porous membranes. *Desalination* **2023**, *547*, 116237−116248.

(30) Lin, B.; Rietveld, L. C.; Yao, L.; Heijman, S. G. J. Adsorption and cake layer fouling in relation to Fenton cleaning of ceramic nanofiltration membranes. *J. Membr. Sci.* **2023**, *687*, No. 122097.

(31) Lv, Z.; Zhang, S.; Jiao, W.; Zuo, X.; Zhang, Y.; Liu, Y. High-efficiency cleaning technology and lifespan prediction for the ceramic membrane treating secondary treated effluent. *Water Sci. Technol.* **2023**, *88* (1), 321−338.
(32) Mo, J.; Lin, T.; Liu, W.; Zhang, Z.; Yan, Y. Cleaning efficiency and mechanism of ozone micro-nano-bubbles on ceramic membrane fouling. *Sep. Purif. Technol.* **2024**, *331*, No. 125698.
(33) Pereira, G. L. D.; Cardozo-Filho, L.; Jegatheesan, V.; Guirardello, R. Generalization and Expansion of the Hermia Model for a Better Understanding of Membrane Fouling. *Membranes* **2023**, *13* (3), 290−336.
(34) Yang, H.; Yu, X.; Liu, J.; Tang, Z.; Huang, T.; Wang, Z.; Zhong, Q.; Long, Z.; Wang, L. A Concise Review of Theoretical Models and Numerical Simulations of Membrane Fouling. *Water* **2022**, *14* (21), 3537−3556.
(35) Fraenkel, D. Correlation between the specific conductivity and the equivalent conductivity of an individual ion in electrolyte solution. *Chem. Phys. Lett.* **2021**, *781*, No. 138957.
(36) Zhong, C.; Wang, Z. A three-mechanism (intermediate pore blocking, standard pore blocking and cake filtration) model considering correction of effective filtration area. *J. Environ. Chem. Eng.* **2024**, *12* (5), No. 113654.
(37) Gul, A.; Hruza, J.; Dvorak, L.; Yalcinkaya, F. Chemical Cleaning Process of Polymeric Nanofibrous Membranes. *Polymers* **2022**, *14* (6), No. 1102.
(38) Chowdhury, S.; Shrivastava, S.; Kakati, A.; Sangwai, J. S. Comprehensive Review on the Role of Surfactants in the Chemical Enhanced Oil Recovery Process. *Ind. Eng. Chem. Res.* **2022**, *61* (1), 21−64.
(39) Meconi, G. M.; Ballard, N.; Asua, J. M.; Zangi, R. Adsorption and desorption behavior of ionic and nonionic surfactants on polymer surfaces. *Soft Matter* **2016**, *12* (48), 9692−9704.
(40) Lee, J.; Zhou, Z.-L.; Behrens, S. H. Interfaces Charged by a Nonionic Surfactant. *J. Phys. Chem. B* **2018**, *122* (22), 6101−6106.
(41) Das, S.; Nguyen, Q.; Patil, P. D.; Yu, W.; Bonnecaze, R. T. Wettability Alteration of Calcite by Nonionic Surfactants. *Langmuir* **2018**, *34* (36), 10650−10658.
(42) Müller, W.; Sroka, W.; Schweins, R.; Nöcker, B.; Poon, J.-F.; Huber, K. Impact of Additive Hydrophilicity on Mixed Dye-Nonionic Surfactant Micelles: Micelle Morphology and Dye Localization. *Langmuir* **2024**, *40* (17), 8872−8885.
(43) Ma, C.; Zhu, X.; Li, W. Extraction and separation of vanadium (IV) by EHEHPA with citric acid complexing iron (III) from sulfate leaching solution. *Sep. Purif. Technol.* **2023**, *316*, No. 123720.
(44) Hao, Y.; Ma, H.; Wang, Q.; Zhu, C.; He, A. Complexation behaviour and removal of organic-Cr(III) complexes from the environment: A review. *Ecotoxicol. Environ. Saf.* **2022**, *240*, No. 113676.
(45) Payehghadr, M.; Hashemi, S. E. Solvent effect on complexation reactions. *J. Inclusion Phenom. Macrocyclic Chem.* **2017**, *89* (3−4), 253−271.
(46) Malenov, D. P.; Zarić, S. D. Chelated metal ions modulate the strength and geometry of stacking interactions: energies and potential energy surfaces for chelate−chelate stacking. *Phys. Chem. Chem. Phys.* **2018**, *20* (20), 14053−14060.
(47) He, H.; Wang, J.; Fei, X.; Wu, D. Sequestration of free and chelated Ni(II) by structural Fe(II): Performance and mechanisms. *Environ. Pollut.* **2022**, *292*, No. 118374.

https://doi.org/10.1021/acsomega.5c01000
ACS Omega 2025, 10, 17917−17928